AGU PUBLICATIONS

JGR

Journal of Geophysical Research: Biogeosciences

RESEARCH ARTICLE
10.1002/2014JG002672

Key Points:
- Ice-covered lakes exhibit spatial variations of UW PAR and chl-a distribution
- UW PAR is negatively correlated with chlorophyll-a

Correspondence to:
M. K. Obryk,
mobryk@pdx.edu

Citation:
Obryk, M. K., P. T. Doran, and J. C. Priscu (2014), The permanent ice cover of Lake Bonney, Antarctica: The influence of thickness and sediment distribution on photosynthetically available radiation and chlorophyll-a distribution in the underlying water column, *J. Geophys. Res. Biogeosci.*, *119*, doi:10.1002/2014JG002672.

Received 20 MAR 2014
Accepted 26 AUG 2014
Accepted article online 30 AUG 2014

The permanent ice cover of Lake Bonney, Antarctica: The influence of thickness and sediment distribution on photosynthetically available radiation and chlorophyll-a distribution in the underlying water column

M. K. Obryk[1], P. T. Doran[1], and J. C. Priscu[2]

[1]Department of Earth and Environmental Sciences, University of Illinois at Chicago, Chicago, Illinois, USA, [2]Department of Land Resources and Environmental Sciences, Montana State University, Bozeman, Montana, USA

Abstract The thick permanent ice cover on the lakes of the McMurdo Dry Valleys, Antarctica, inhibits spatial lake sampling due to logistical constraints of penetrating the ice cover. To date most sampling of these lakes has been made at only a few sites with the assumption that there is a spatial homogeneity of the physical and biogeochemical properties of the ice cover and the water column at any given depth. To test this underlying assumption, an autonomous underwater vehicle (AUV) was deployed in Lake Bonney, Taylor Valley. Measurements were obtained over the course of 2 years in a 100 × 100 m horizontal sampling grid (at a 0.2 m vertical resolution). Additionally, the AUV measured the ice thickness (in water equivalent) and collected images looking up through the ice, which were used to quantify sediment distribution on the surface and within the ice. Satellite imagery was used to map sediment distribution on the surface of the ice. We present results of the spatial investigation of the sediment distribution on the ice cover and its effects on biological processes, with particular emphasis on photosynthetically active radiation (PAR). The surface sediment is a secondary controller of the ice cover thickness, which in turn controls the depth-integrated PAR in the water column. Our data revealed that depth-integrated PAR was negatively correlated with depth-integrated chlorophyll-a ($r = 0.88$, $p < 0.001$, $n = 83$), which appears to be related to short-term photoadaptation of phytoplanktonic communities to spatial and temporal variation in PAR within the water column.

1. Introduction

Lake sampling of Antarctic perennially ice-covered lakes is usually limited to only a few sites per year because of the challenge of getting access to the water column. Sampling is usually performed at the deepest part of the lake, which is assumed to represent the entire lake at any given depth. Such an assumption might be valid in temperate lakes due to the seasonal overturning of the water column. However, because of the strong stratification and lack of mixing in the Antarctic lakes [*Spigel and Priscu*, 1998], biogeochemical horizontal homogeneity of the water column might not exist. The low kinetic energy of the Antarctic lake systems (diffusion dominates the spatial transport of constituents) may produce an ecosystem and ecosystem limits that vary significantly in three dimensions, variations which will not be detected with lake data sets collected at one site at various depths. *Spigel and Priscu* [1998] have shown spatial and temporal stability of the water column based on 3 years of conductivity and temperature profiles in perennially ice-covered Lake Bonney (Figure 1). However, variations of underwater photosynthetically active radiation (UW PAR) and chlorophyll-a under the ice have not been previously documented in high spatial and temporal resolution.

In this paper, we present the results of an investigation by the Environmentally Non-Disturbing Under-ice Robotic ANtarctiC Explorer (ENDURANCE), deployed during the 2008/2009 and 2009/2010 seasons, with the objective of testing autonomous technologies for the under-ice exploration of icy moons such as Europa [*Stone et al.*, 2010]. We tested whether UW PAR and chlorophyll-a are spatially stable using data collected by an autonomous underwater vehicle (AUV), which was deployed in the west lobe of Lake Bonney, Taylor Valley, McMurdo Dry Valleys to perform a high-resolution spatial and temporal biogeochemical and physical survey of the entire lake (Figure 1). Spatial patterns of sediment distribution, both on the surface and within

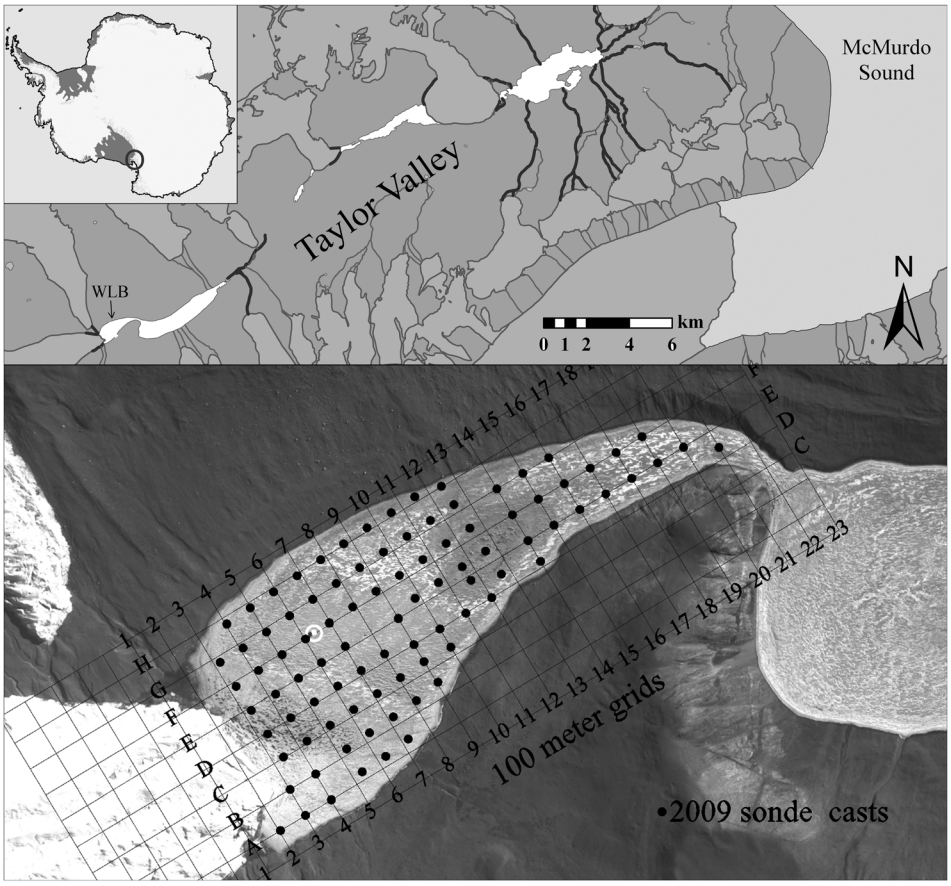

Figure 1. (top) Map of the lakes located in the Taylor Valley. (bottom) Satellite image of west lobe of Lake Bonney with an overlaid 100 × 100 m grid. Black dots represent sampling locations during 2009/2010 season. Satellite image was obtained from DigitalGlobe ™ (shot on 6 December 2008) and processed by the Polar Geospatial Center.

the ice cover, and the effects of this sediment distribution on sub-ice processes are discussed. In particular, this paper focuses on the ice cover properties and their effects on photosynthetically active radiation and the spatial distribution of chlorophyll-a in the lake.

1.1. Study Site

Taylor Valley, McMurdo Dry Valleys contains several perennially ice-covered lakes located in hydraulically closed basins. The McMurdo Dry Valleys are predominantly ice free, as the Transantarctic Mountains effectively block the down valley flow of the continental ice sheet. The main source of water for most lakes is from local alpine glaciers. The exception is Lake Bonney, which receives inflows from the Taylor Glacier, an outlet glacier from the Polar Plateau. These glaciers melt during the short austral summers, producing ephemeral streams that feed into the lakes. All Taylor Valley lakes have perennially frozen ice covers that prohibit wind-driven turbulence and its associated mixing of water [*Spigel and Priscu*, 1998]. The ice cover thickness in all Taylor Valley lakes fluctuates between 3 and 6 m [*Doran et al*., 2002; *McKay et al*., 1985]. The mean annual ablation of the ice cover in Taylor Valley lakes varies between 0.64 m and 0.99 m, and as such, the residence of lake ice ranges between 3 and 5 years [*Dugan et al*., 2013]. The growth of the ice from the bottom down results in ice crystal growth with a vertical *c* axis, permitting sufficient penetration of solar radiation to support phototrophic life [*Chinn*, 1993]. The lakes exhibit a strong vertical gradient of salinity, a unique pattern of thermal stratification, and a deep chlorophyll maximum [*Lizotte and Priscu*, 1994; *Spigel et al*., 1991; *Vincent et al*., 2008]. The source of heat trapped in the liquid water column comes from solar radiation through the ice cover during the austral summer, stream inflow, and latent heat of ice formation [*McKay et al*., 1985; *Wilson*, 1981].

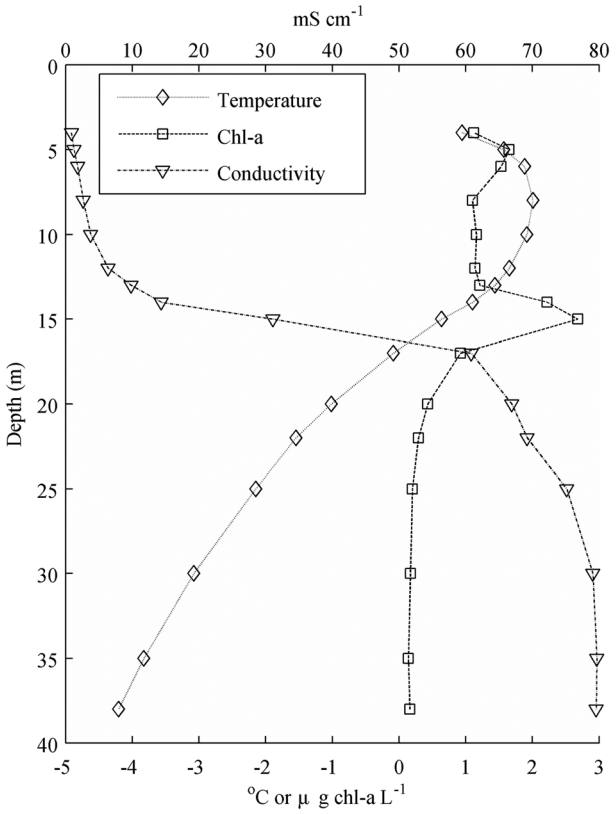

Figure 2. West lobe of Lake Bonney, profiles in November 2009. Data are obtained from www.mcmlter.org. Resolution of temperature and conductivity data was reduced to match resolution of chlorophyll-a measurements.

Lake Bonney is situated in the upper part of the Taylor Valley, 27 km from the coast (Figure 1). The lake is divided into two separate lobes (east and west) that are connected by a shallow, narrow channel. The west lobe of Lake Bonney (WLB) is approximately 2.6 km in length and 0.9 km in width [*Chinn*, 1993]. The WLB abuts Taylor Glacier on its westernmost side and connects with the east lobe of Lake Bonney on the eastern side through a narrow channel (Figure 1). The typical profiles of the water column in the west lobe of Lake Bonney (as shown in Figure 2) illustrate the sharp thermal and chemical stratification of this lake [*Spigel and Priscu*, 1998]. The change in conductivity indicates a chemocline at a depth of approximately 15 m (Figure 2). The distinct salt gradient is responsible for controlling mixing of the water column, with temperature exerting very little influence on density, permitting unique stable ecosystem to develop [*Lizotte and Priscu*, 1992; *Spigel and Priscu*, 1998]. Phytoplankton in the fresh water column ($<$15 m depth) is shade adapted and nutrient limited due to light attenuation by the thick ice cover and lack of vertical water mixing, respectively [*Lizotte and Priscu*, 1992; *Lizotte et al*., 1996]. Chlorophyll-a peaks at the chemocline (deep chlorophyll-a maximum) due to the diffuse upwelling of nutrients from deep nutrient-rich waters [*Priscu*, 1995; *Spigel and Priscu*, 1998].

2. Methods

2.1. Navigation of the Autonomous Underwater Vehicle

The AUV was designed to swim under the ice cover at a fixed shallow depth (generally 5 m below the piezometric water level). At predefined intervals, the AUV would stop, ascend, and prop itself against the bottom of the ice cover (a process herein termed ice picking), at which time it would lower a sensor-equipped sonde. The sonde collected continuous data throughout the water column to the bottom of the lake. It profiled at 2 Hz with a typical decent speed of 0.4 m s^{-1}, which translates into a measurement every 0.2 m. This design eliminated the need for the vehicle to swim through the entire volume of the lake to collect data thereby minimizing disturbance of the water column of Lake Bonney.

Navigation under a thick ice cover poses a challenge. The only access to the surface is via the entry melt hole in the lake ice. The ENDURANCE navigation system was composed of three hierarchical subsystems (dead reckoning, acoustic beacon, and visual homing) to allow successful mission deployment and the return of the AUV to the melt hole [*Stone et al*., 2010]. The main navigation was performed with a dead-reckoning subsystem that included a ring laser gyroscope inertial unit for vehicle orientation, two pressure transducers for depth determination, and a Doppler velocity log for velocity detection through bottom tracking [*Stone et al*., 2010]. The integration of these components allowed the AUV to determine its position based on its own velocity and orientation with high precision. This navigation system typically returned the vehicle directly under the deployment hole at the end of each mission. Once beneath the deployment hole, the vehicle would track a light shined down the hole and ascend to the surface. In case of a power failure, the AUV was

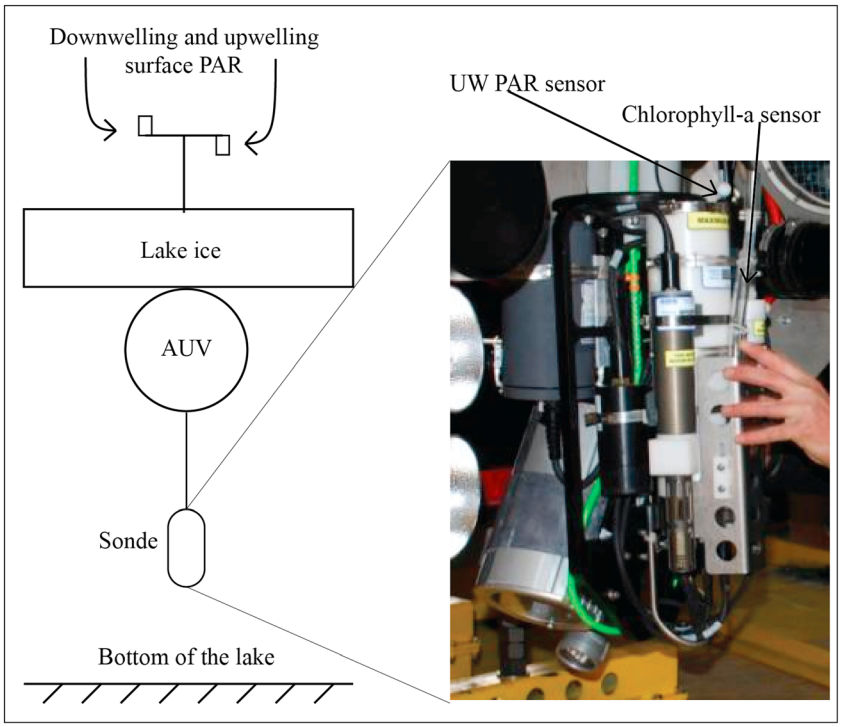

Figure 3. Schematic representation of the Autonomous Underwater Vehicle (AUV) sampling (ice picking) at west lobe of Lake Bonney. During the ice picking, the AUV was motionless, pressing itself against the bottom of the ice, at which point it lowered a sensor-equipped sonde. Simultaneous downwelling and upwelling photosynthetically active radiation was obtained on the surface of the ice by people tracking the vehicle.

equipped with a magnetic field generator, which allowed us to locate the vehicle under the ice using a phase-locked loop receiver (beaconing device) [*Stone et al*., 2010]. However, this recovery system proved to be a powerful tool in precisely georeferencing the location of the vehicle during ice picking. Thus, each sampling location was recorded on the surface with a high-resolution real-time kinematic differential GPS unit. The accuracy of our positioning using this method is on the order of centimeters.

Measurements were taken in a 100 × 100 m grid across the entire lake (higher-density sampling was performed near the snout of the Taylor Glacier), generating high-resolution spatial data. During the 2008/2009 season, 44 locations were sampled during 19 dives from 5 December to 24 December, covering the western half of the WLB. During the 2009/2010 season, 83 locations (used in this study) were sampled over 11 days from 6 November to 17 November, representing the entire lake (Figure 1). After each "mission," the AUV obtained measurements from one location (F6—located near the deployment hole), which was designated to serve as a control point to observe temporal change in the lake. The temporal data were obtained from 9 November to 2 December during the 2009/2010 season, generating 12 profiles.

2.2. Sonde and Vehicle Instruments

The AUV was outfitted with scientific instruments that were attached to the sonde, which was attached to the vehicle by a cable wound on a spooler drum (Figure 3). The sonde, equipped with sensors for depth (Digi-Quartz pressure transducer), conductivity, temperature, underwater photosynthetically active radiation, turbidity and chlorophyll-a fluorescence, colored dissolved organic matter (CDOM), pH, and reduction-oxidation, was lowered to the bottom of the lake during ice-picking maneuvers. Conductivity, temperature, and pressure were collected using a SEACAT conductivity-temperature-depth profiler (SBE 19*plus* v2). We provide details on UW PAR, chlorophyll-a, and turbidity sensors only, which generated data for this paper. Underwater PAR (400 nm to 700 nm) was collected using a Biospherical QSP-2300 spherical 3.7π steradians sensor mounted on top of the sonde to provide a clear field of view when the sonde is deployed (Figure 3). Chlorophyll-a and turbidity were estimated using a WETLAB combination fluorometer FLNTU(RT) sensor.

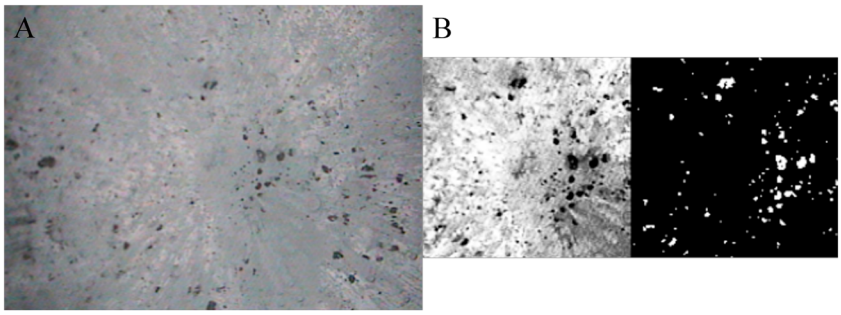

Figure 4. An example of upward looking image that was captured with a camera installed on the top of the autonomous underwater vehicle. The images were used to quantify internal sediment within the ice cover. (a) Original image obtained with the camera. (b) Image processing, which involved cropping the image, conversion to gray scale, enhancement of sediment (left panel), and conversion to black and white to count the pixels representing the sediment (right panel).

Chlorophyll-a fluorescence was measured via excitation at 470 nm and emission at 695 nm, whereas turbidity was measured at 700 nm, avoiding the effect of CDOM interference. In addition, the AUV collected thousands of images looking up through the ice using a Tritech Osprey high-resolution color underwater camera that was installed on top of the AUV [*Stone et al.*, 2010]. The upward looking images were recorded at ~1 Hz; however, only images obtained during ice picking were used in this analysis.

2.3. Surface Photosynthetically Active Radiation

Surface PAR measurements (upwelling and downwelling) were obtained by manually tracking the vehicle from above. While the vehicle was stationary and ice picking two LiCor Li-190 2π quantum PAR sensors were deployed, mounted on a frame with two horizontal outriggers, at the end of which sensors were located in a manner to avoid shading (Figure 3). Fifty-four surface PAR measurements were obtained during the 2009/2010 season. The simultaneous measurement of surface and UW PAR permitted calculations of percentage of PAR transmittance through the ice cover as well as ice surface albedo. Percentage of PAR transmittance normalizes diurnal and seasonal climatic variations throughout the season such as cloudiness, shading by nearby mountains, and increased incident radiation over the 2 weeks when the data were collected.

2.4. Data Processing

2.4.1. Ice Thickness

When the AUV was motionless during ice picking, the initial measurement obtained with the depth sensor (pressure transducer), minus the offset from the sensor's location to the top of the AUV (bottom of the ice), was equal to the measurement of the ice thickness at that point with reference to the hydrostatic water surface. The hydrostatic level indicates where the water would be if a hole were drilled in the ice, and it is assumed to be the thickness of the ice in water equivalent. Sediment load both on the surface and within the ice, and air bubbles within the ice will account for some buoyancy variation in the ice cover.

2.4.2. Internal Sediment

Images obtained using the upward looking camera at georeferenced ice-picking stations were used to quantify sediment distribution within the ice cover. The angular view of the camera in the water is 65 by 50°. The images were cropped, eliminating the optical distortion along the outer perimeter of the image due to the wide field of view. A method for batch image processing was developed using a custom written MATLAB ® script to extract sediment data. The technique involved converting the images to gray scale, enhancing the image's contrast by equalizing the histogram, selecting appropriate threshold values to enhance the sediment in the image, and, finally, converting it to a binary image (black and white) to count the pixels representing the sediment (Figure 4). Pixels were converted to square meters based on the field of view of the camera, which is a function of the ice thickness; i.e., image size is dependent on the thickness of the ice cover (thicker the ice cover, the lesser the resolution). The image processing only allowed quantification of sediment trapped within the ice cover; it does not include sediment on the surface.

Table 1. Summary of Principal Component Analysis Including Loadings of the First Three Principal Components (PCs) and Variance Explained

	PC 1	PC 2	PC 3
Depth-integrated chlorophyll-a	−0.53	0.10	0.06
Depth-integrated UW PAR	0.56	0.06	0.06
Internal sediment	−0.13	−0.78	0.01
Ice thickness (in 2009/2010)	−0.42	−0.35	−0.16
Diffuse attenuation coefficient (K_{PAR})	−0.30	0.21	0.84
% of PAR transmittance at 10 m depth	0.36	−0.47	0.51
Variance explained (%)	48.7	22.9	14.9

2.4.3. Underwater PAR, Chlorophyll-a, and Diffuse Attenuation Coefficient

Depth-integrated underwater PAR and chlorophyll-a were calculated over the 6 to 10 m depth interval. This depth range was selected because (1) the AUV casts a shadow over the PAR sensor on the sonde down to a 6 m depth, (2) to allow inclusion of most of the lake regardless of total depth, and (3) to avoid possible self-shading of the underwater PAR due to the deep chlorophyll-a maximum (attenuation of light due to an increased biomass) which occurs at ~15 m. The shading effect by the AUV was determined by investigating UW PAR data in the water column based on all measured profiles. The observed increase of UW PAR, with depth, between the first measurements obtained during the ice picking down to 6 m depth is indicative of the AUV casting a shadow on the sonde and its associated instruments.

Depth-integrated UW PAR was not corrected for the changes in the incident PAR because of limited overlapping surface PAR measurements. However, we found that % of PAR transmittance at 10 m depth (which is corrected for incident PAR) and depth-integrated UW PAR are positively correlated ($r = 0.54$, $p < 0.001$, $n = 54$). The low correlation coefficient is a result of mountains casting a shadow on the northern side of the lake (half of the lake).

Diffuse attenuation coefficient (K_{PAR}) was calculated using a ratio of UW PAR irradiance at 6 and 10 m depth: $K_{PAR} = \ln[E(z_6) \times E(z_{10})^{-1}] \times \Delta z^{-1}$, where E is measured UW PAR at depth z.

2.4.4. Statistical Analysis

Principal component analysis (PCA) was employed because of the large number of variables used in this study. PCA was used to discern trends and patterns in the data, with the first components explaining the majority of the variance. The variables included in the PCA are depth-integrated chlorophyll-a, depth-integrated UW PAR, K_{PAR}, ice thickness, internal sediment, and percentage of PAR transmittance at 10 m depth. However, since percentage of PAR transmittance (% PAR) was only calculated at 54 ice-picking locations, ice-picking locations of all the other variables that correspond to the missing stations of % PAR were deleted in order to produce a gapless 54 × 6 matrix. Where, 54 is a number of ice-picking locations and 6 is number of variables. Because all variables are in different units, PCA was performed using the inverse variances of the data as the weights, in order to normalize the data set. Upon interpretation of the PCs, Pearson's linear correlation coefficients were determined between variables in question.

3. Results

3.1. Principal Component Analysis

The first three principal components explain 48.7, 22.9, and 14.9% of variance, respectively (Table 1 and Figure 5). PC 1 describes a relationship between PAR (both depth integrated and % of PAR transmittance), depth-integrated chlorophyll-a, and ice thickness, where PAR is negatively correlated with chlorophyll-a and ice thickness. PC 2 is concerned with the effect of internal sediment on % of PAR transmittance. Finally, PC 3 shows a relationship between K_{PAR}, % of PAR transmittance (Figure 5). Statistically significant linear correlations between the trends observed by the PCA are explored below.

3.2. Ice Thickness

Data obtained from the ice picking show large spatial variations in the ice thickness across the west lobe (Figures 6a and 6b). The northern side of the lake shows pronounced thickening of the ice by about 70 cm compared with the southern side. In addition, the ice cover exhibits two distinct regions of ice thinning on

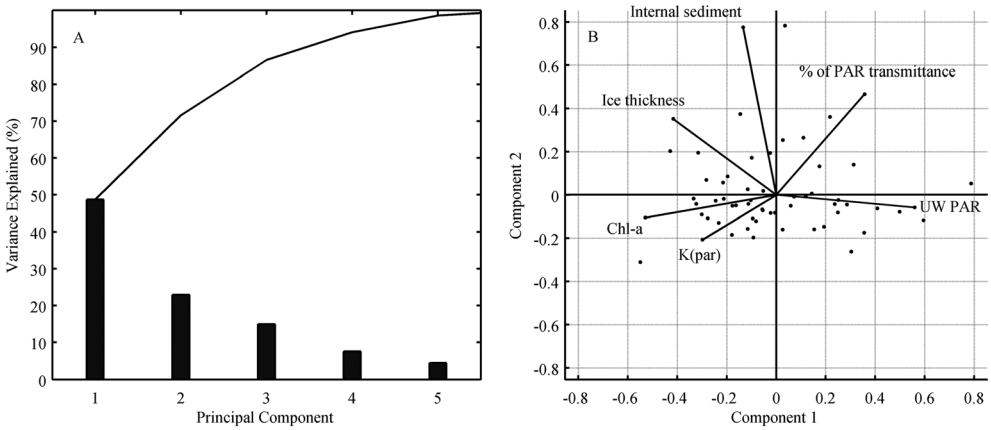

Figure 5. (a) Scree plot of variance explained by the principal component analysis (PCA) and (b) a biplot of loadings and scores for each variable, where K_{PAR} is diffuse attenuation coefficient, Chl-a is depth-integrated chlorophyll-a, and UW PAR is depth-integrated underwater photosynthetically active radiation for data obtained during the 2009/2010 season.

the southwest side of the lake, where the lake abuts Taylor Glacier, and in the east central portion of the lake (Figure 6b). The two localized regions of thinner ice cover are associated with aeolian sediment deposition on the surface of the ice, as shown by a comparison with high-resolution satellite imagery (Figure 7).

A comparison of historical aerial and satellite imagery (dating to 1958) of the west lobe of Lake Bonney reveals that the distribution of the sediment on the surface of the ice cover is a persistent feature of this lake, especially the sediment on the west side along the glacier. All images show aeolian sediment deposition along the glacier face of the lake with small spatial variations (data obtained from Polar Geospatial Center: www.agic.umn.edu). The oval center-east region of the surface sediment accumulation appears to be relatively new and has been present for less than a decade.

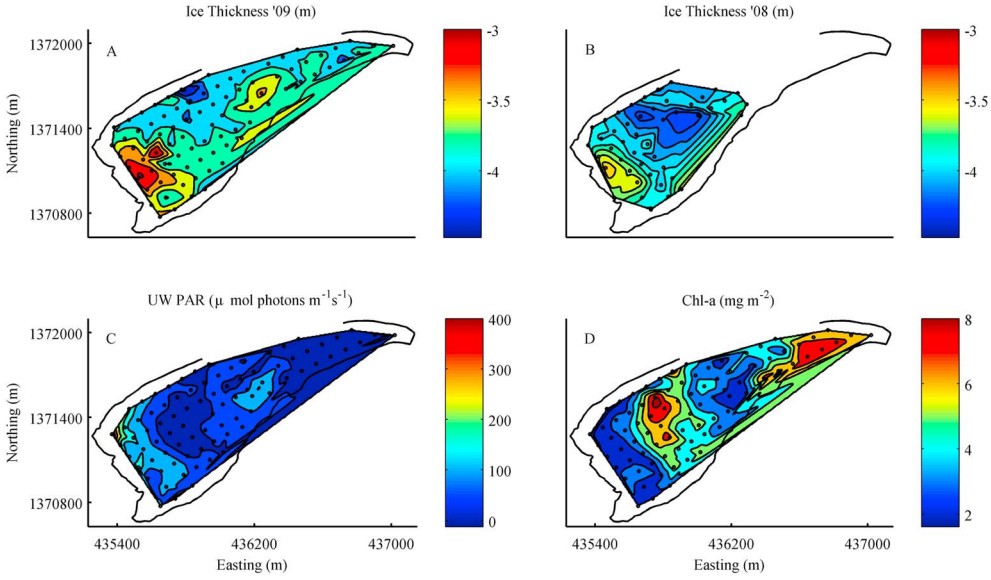

Figure 6. Spatial ice thickness variations (in water equivalent) of west lobe of Lake Bonney during the (a) 2009/2010 and (b) 2008/2009 seasons. (c) Depth-integrated (from 6 to 10 m) underwater photosynthetically active radiation (2009/2010 season). (d) Depth-integrated (from 6 to 10 m) chlorophyll-a (2009/2010 season). All maps are projected in universal transverse Mercator (UTM) coordinates. Black contour represents the west lobe of Lake Bonney parameter obtained with high-resolution GPS. Dots represent locations of data collection.

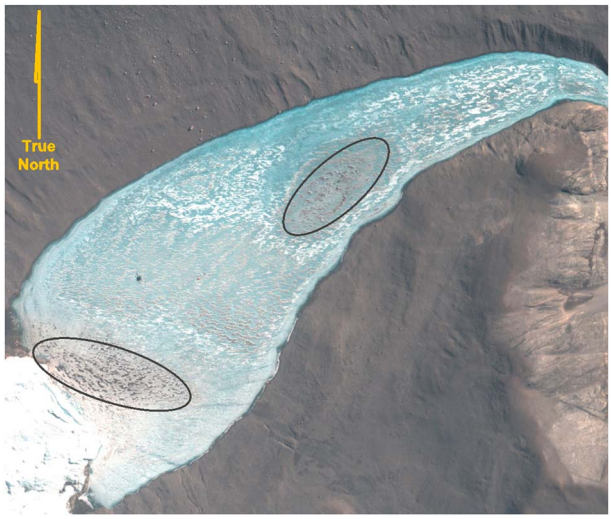

Figure 7. High-resolution satellite image of west lobe of Lake Bonney. The circled regions represent aeolian sediment accumulated on the surface of the ice cover, associated with thinner ice cover. Quickbird satellite image was obtained from DigitalGlobe ™ (shot on 6 December 2008) and processed by Polar Geospatial Center.

The spatial ice thickness variations during the 2009/2010 season are 1.4 m, with a maximum value of 4.4 m on the north side of the lake and a minimum value of 3.0 m by the glacial face where aeolian sediment accumulates on the surface of the ice cover (average ice thickness = 3.7, $\sigma = 0.23$ (Figure 6a)). The ice thickness data from the 2008/2009 season only cover the western half of the lake; however, the spatial ice thickness distribution was similar to that in the 2009/2010 season (Figures 6a and 6b). Extensive thinning of the ice was observed along the glacier, where aeolian sediment had accumulated, with a minimum value of 3.5 m. A temporal comparison of the ice cover thickness between all overlapping data points (representing the western half of the lake) for the two seasons shows an average ice cover loss of 0.22 m ($\sigma = 0.23$, min = -0.94, max = 0.52) over a period of 1 year despite the decrease of winter temperature (March to September) by 0.9°C between the two seasons.

3.3. Sediment Within the Ice

Images obtained with the upward looking camera show that sediment accumulates in small discrete patches or lenses. The surface area of entrapped sediment ranges from 0.00 to 0.12 m^2. *Adams et al.* [1998] reported sediment pockets that are several centimeters across, based on the ice cores recovered from WLB. However, the ice cores are only 10 cm in diameter [*Adams et al.*, 1998]; hence, they will underestimate surface area calculations and cannot be compared with our results. The spatial distribution of entrapped sediment patches varies widely across the lake (Figure 8a) and shows a statistically significant, linear correlation with ice thickness ($r = 0.32$, $p = 0.005$, $n = 76$), depth-integrated UW PAR ($r = -0.25$, $p = 0.029$, $n = 74$), and % of PAR transmittance at 10 m depth ($r = 0.28$, $p = 0.041$, $n = 54$). Percentage of PAR transmittance at 10 m depth is shown in Figure 8b. It is noteworthy that although no images were recorded from the AUV's forward looking camera, we did observe in real-time sediment patches at the very bottom of the ice cover. The existence of these patches is not explained by any ice/sediment models developed to date [e.g., *Jepsen et al.*, 2010; *Simmons et al.*, 1986].

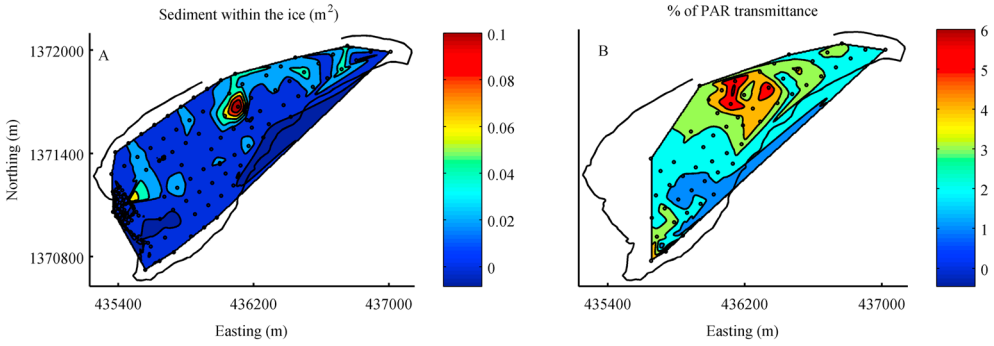

Figure 8. (a) Spatial variations of sediment incorporated within the ice and (b) percentage of light transmittance at 10 m depth for sample locations during the 2009/2010 season. Maps are projected in UTM coordinates. Black contour represents the west lobe of Lake Bonney parameter. Dots represent locations of data collection.

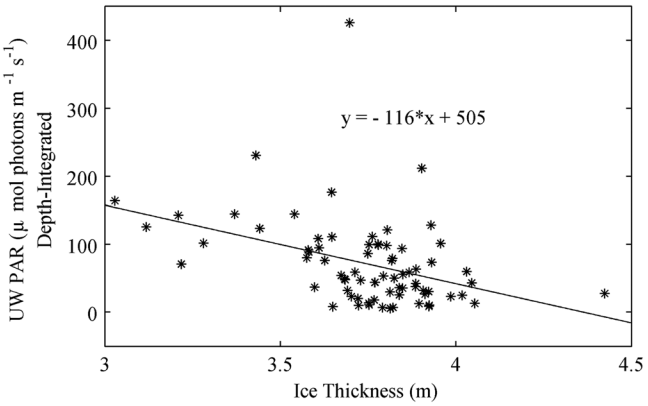

Figure 9. Depth-integrated underwater photosynthetically active radiation versus ice thickness ($r = -0.40$, $p < 0.001$, $n = 83$) for all sample locations during the 2009/2010 season.

3.4. PAR, K_{PAR}, and Turbidity

Depth-integrated UW PAR (from 6 to 10 m) shows two pronounced regions of greater light in the water column: along the glacier face (west side of the lake), extending roughly 300 m eastward from the glacier, and the center-east side of the lake (Figure 6c). The maximum values of depth-integrated UW PAR are found on the northwestern edge of the lake (425.8 μmol photons m^{-1} s^{-1}), with minimum values on the far eastern end of the lake (5.6 μmol photons m^{-1} s^{-1}). The relationship between ice thickness and depth-integrated UW PAR yields a poor yet statistically significant negative linear correlation ($r = -0.40$, $p < 0.001$, $n = 83$) (Figures 6a, 6c, and 9).

Diffuse attenuation coefficient positively correlates with depth-integrated chlorophyll-a ($r = 0.39$, $p < 0.001$, $n = 83$) and negatively with depth-integrated UW PAR ($r = -0.33$, $p < 0.001$, $n = 83$). The water column of the WLB has extremely low turbidity (Figure 10), and no statistically significant correlations were found between turbidity and chlorophyll-a or turbidity and underwater PAR.

3.5. Chlorophyll-a

Depth-integrated chlorophyll-a (from 6 to 10 m, which is above the deep chlorophyll-a maximum) is the highest on the east side of the lake near the narrows (7.9 mg m^{-2}), where the lake merges and connects with the east lobe of Lake Bonney (Figure 6d). The smallest chlorophyll-a concentration is along the glacier interface (1.6 mg m^{-2}). The linear correlation coefficient was calculated between spatial log-transformed depth-integrated UW PAR and depth-integrated chlorophyll-a ($r = -0.89$, $p < 0.001$, $n = 83$) (Figure 11) and % of PAR transmittance at 10 m depth and depth-integrated chlorophyll-a ($r = -0.50$, $p < 0.001$, $n = 54$). The time series of depth-integrated UW PAR and depth-integrated chlorophyll-a also show a negative correlation ($r = -0.87$, $p < 0.001$, $n = 12$) (Figure 12). In addition, ice thickness and depth-integrated chlorophyll-a show a statistically significant linear correlation ($r = 0.40$, $p < 0.001$, $n = 83$).

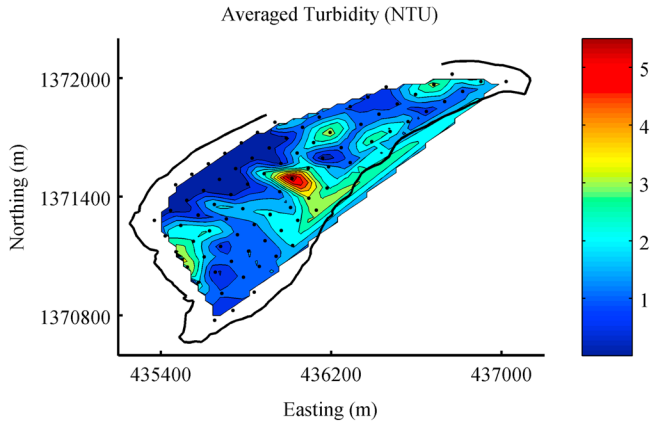

Figure 10. Averaged turbidity between 6 and 10 m depth for all sample locations during the 2009/2010 season. Map is projected in UTM coordinates. Black contour represents the west lobe of Lake Bonney parameter. Dots represent locations of data collection.

4. Discussion

Analyses of the high-resolution spatial data from the west lobe of Lake Bonney revealed ice thinning along the Taylor Glacier face and the central east side of the lake. These two pronounced regions of thin ice cover are associated with the accumulation of aeolian sediment (Figures 6a and 7) which can enhance thinning due to the absorption of incident solar radiation by the surface sediment during the austral summer months [*Jepsen et al.*, 2010]. Variations in spatial distribution of surface sediments have been attributed to the strength of the winter winds,

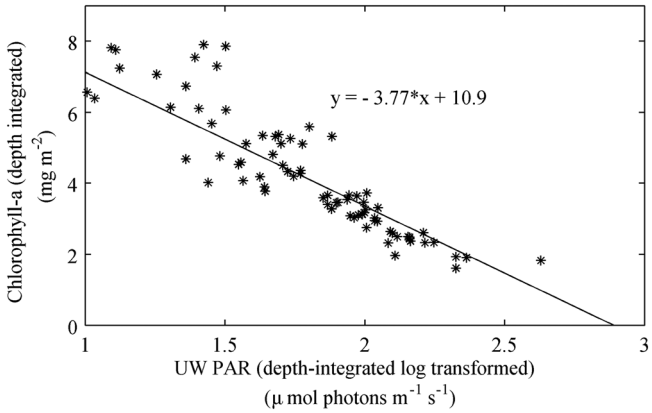

Figure 11. Log-transformed underwater photosynthetically active radiation (UW PAR) versus chlorophyll-a ($r = -0.88$, $p < 0.001$, $n = 83$) for all sample locations during the 2009/2010 season. Both UW PAR and chlorophyll-a are depth-integrated from 6 m to 10 m at each sample location.

during which most of the wind-blown sediment accumulates [*Priscu et al.*, 1998]. However, the analysis of historic aerial and satellite images reveals the apparent static nature of the sediment accumulation on the ice, especially along the glacier face, suggesting that the spatial pattern of the ice cover thickness of the west lobe of Lake Bonney has remained the same for several decades. Conversely, the thicker ice cover on the north side of the lake presumably results from shading by mountains to the north of the lake, which is most pronounced near solar noon [*Dana et al.*, 1998]. Decrease in solar radiation will, in turn, decrease ablation during the summer months [*Clow et al.*, 1988; *Dana et al.*, 1998; *McKay et al.*, 1985]. Our data imply that accumulation of aeolian sediment on the surface of the ice cover and localized shading play a major role in controlling the ice cover thickness at small scales.

Ice cover thickness is positively correlated with sediment incorporated within the ice. This presents an apparent paradox as thinner ice cover contains a lesser amount of internal sediment, yet thinner ice is associated with aeolian sediment accumulation on the surface of the ice cover. Field studies and an energy balance model show that surface sediment can propagate through the ice to 2 m depth [*Jepsen et al.*, 2010]. The release of subsurface sediment from this depth occurs during the austral summers when the ice becomes unstable and permeable, forming vertical cracks that allow for downward movement of sediment [*Jepsen et al.*, 2010; *Nedell et al.*, 1987; *Squyres et al.*, 1991]. However, *Jepsen et al.* [2010] proposed that the differences in the ice thickness can cause a rapid rebound of thinner ice that can generate cracks and fractures in the ice. The associated cracks become conduits for any subsurface sediment to be released from the ice into the water column [*Jepsen et al.*, 2010; *Nedell et al.*, 1987; *Squyres et al.*, 1991]. The weak positive relation between internal sediment and ice thickness is a result of longer residence of the internal sediment within thicker ice cover.

Water column, depth-integrated PAR is associated with variations of the ice thickness; i.e., thicker ice cover results in a lesser amount of depth-integrated PAR. The aeolian sediment accumulation on the surface of the ice cover has a pronounced effect on the thinning of the ice (up to 1 m) due to the absorption of the solar energy by the sediment, which increases ablation at the surface (Figures 6a and 7). Light transmittance through the ice has been characterized by dividing the ice into discrete horizontal layers that have distinct optical properties [*Fritsen and Priscu*, 1999; *McKay et al.*, 1994]. The majority of the light is absorbed and scattered at the very top layer of the ice (up to 1 m depth) because of morphologically distorted air bubbles, Tyndall figures (disks of liquid water resulting from the internal melting of ice), ice whitening, and entrapped sediment [*Fritsen and Priscu*, 1999; *McKay et al.*, 1994].

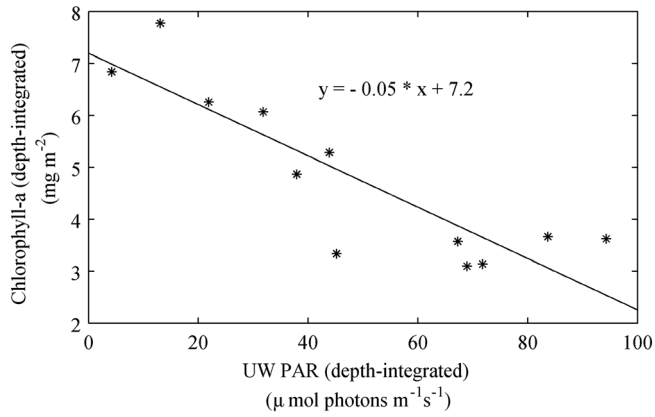

Figure 12. Underwater photosynthetically active radiation (UW PAR) versus chlorophyll-a ($r = -0.87$, $p < 0.001$, $n = 12$) representing temporal data from 9 November 2009 to 2 December 2009, obtained from F6 location. Both UW PAR and chlorophyll-a are depth-integrated from 6 m to 10 m at each sample location.

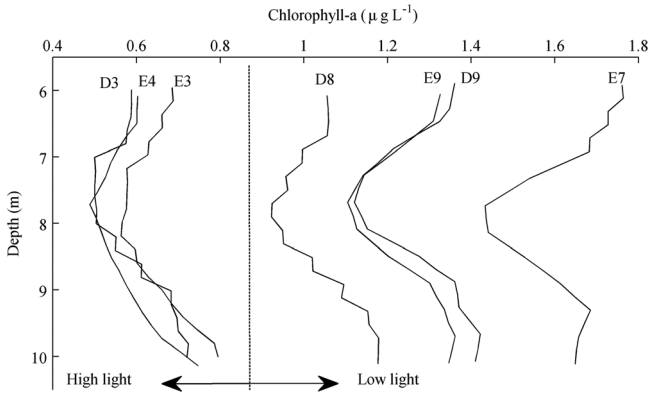

Figure 13. An example of chlorophyll-a profiles (from 6 m to 10 m) under two different light regimes in the west lobe of Lake Bonney from 2009/2010 data set. For clarity, only a few selected profiles are plotted. Profile names correspond with their location in Figure 1.

The homogeneous clear bottom layer of the ice cover is assumed to be winter growth with vertical chains of undisturbed air bubbles [*Adams et al*., 1998; *McKay et al*., 1994]. The subsurface sediment accumulates in small discrete patches at 2 m depth below morphologically disturbed ice (example Figure 4); as a result, it has little impact on PAR transmittance (based on the decreasing diffuse attenuation coefficient with depth within the ice [*Fritsen and Priscu*, 1999]). Hence, the top meter of the ice alone plays a major role in controlling the total available PAR in the water column [*Fritsen and Priscu*, 1999]. The surface sediment is responsible for the increased ablation of the ice (hence thinner ice) by removing the morphologically disturbed layer (top 1 m) and allowing more light penetration. We suggest that the surface area of internal sediment patches is too small to interfere with the penetrating light. However, it is interesting to note that PC 2 and a linear correlation show a positive relationship between the subsurface sediment and % of PAR transmittance. This relationship does not demonstrate causation, as we have shown above that the internal sediment is associated with thicker ice cover, which attenuates penetrating light.

Our data show that depth-integrated UW PAR is negatively correlated with depth-integrated chlorophyll-a (Figures 6c, 6d, 11 and 12 and Table 1). This negative correlation presents a paradox, as the long-term analysis (over the course of multiple austral summers) of PAR and chlorophyll-a in the WLB shows positive trends [*Fritsen and Priscu*, 1999]. Increased phytoplankton biomass during early spring in WLB has been shown to be stimulated by an increase in incident irradiance [*Lizotte et al*., 1996].

The negative relationship between chlorophyll-a and underwater PAR could be attributed to self-shading, where a high concentration of biomass at the deep chlorophyll-a maximum will attenuate light at and below it. However, WLB is a relatively low-productivity lake, and the deep chlorophyll-a maximum has been shown not to influence light transmittance significantly [*Lizotte and Priscu*, 1992]. Moreover, this study is focused on the shallow fresh waters of WLB (6 to 10 m depth), where very low chlorophyll-a concentrations exist (Figure 13). Furthermore, self-shading would manifest itself in an increased diffuse attenuation coefficient (K_{PAR}) at the sites with lowered underwater PAR, as a result of an increased biomass (increased biomass would attenuate light). We report a statistically significant correlation between chlorophyll-a and K_{PAR}; however, this relationship only accounts for 15% of variance.

Chlorophyll fluorescence can be used to estimate chlorophyll-a concentration and primary productivity [*Lizotte and Priscu*, 1992]. However, the negative correlation we observed between chlorophyll-a and underwater PAR is not necessarily indicative of biomass changes. Rather, it presumably reflects changes in chlorophyll-a concentration per cell. Collectively, our data imply that the negative relationship we observed between chlorophyll-a and under ice PAR in WLB is the result of short-term photoadaptation of phytoplanktonic communities living in the water column. Photoautotrophic organisms living in the Antarctic lakes are highly shade adapted, and they have a variety of mechanisms to cope with low light [*Lizotte and Priscu*, 1992; *Morgan-Kiss et al*., 2006; *Neale and Priscu*, 1995]. One of the short-term techniques of photoadaptation is a change in light-harvesting antenna size with respect to available light [*Morgan-Kiss et al*., 2006]. During low irradiance, phytoplankton will increase chlorophyll-a per unit cell to compensate for the lack of available light to meet their energy requirements [*Miskiewicz et al*., 2000; *Morgan-Kiss et al*., 2006]. Such adaptations have been observed in fresh water lakes on the southern part of the Soya Coast, East Antarctica [*Tanabe et al*., 2008], and in Ariake Bay, Japan [*Shibata et al*., 2010], and have been discussed for Lake Bonney by *Neale and Priscu* [1995], *Lizotte and Priscu* [1992], and *Kong et al*. [2014]. These reports in concert with our data indicate that cell specific changes in chlorophyll-a in response to variations in under-ice

PAR may produce the trends shown in our data (Figures 6d, 11, and 12). The temporal analysis suggests that the observed negative correlation persists throughout the season.

5. Conclusions

Owing to the logistical difficulties of drilling through the permanent ice covers, studies of perennially ice-covered lakes in Antarctica have typically assumed biogeophysical homogeneity of the lakes, an assumption that is refuted here. Rather, our data indicate that spatially variable ice thickness of perennially ice-covered lakes influences chlorophyll-a concentration of phytoplanktonic communities depending on the available light field. Spatial and short-term temporal changes in bulk chlorophyll-a concentration (based on fluorometeric estimation) are inversely correlated to under ice PAR, presumably because chlorophyll-a per unit cell increases in response to low PAR conditions. We presume that similar patterns occur in other perennially ice-covered lakes, and we caution interpretation of point-based limnological analysis when determining basin wide estimates.

The study of permanently ice-covered polar lakes is hindered by the lack of spatial under-ice data and high-density sampling over time. Our use of an AUV to collect high-resolution spatial data has allowed us, for the first time, to examine the three-dimensional structure of selected physical and biological variables in an Antarctic lake. Together with satellite imagery, we show that sediment accumulation on the surface of the ice controls water column PAR, which in turn can influence the spatial distribution of chlorophyll-a within the near surface water column. Phytoplanktonic communities in the water column are highly shade adapted, and we show here their short-term photoadaptation to changes in the light field based on in vivo fluorescence.

Acknowledgments
The data for this paper are available upon request from the author. Data supporting Figure 2 are available at McMurdo Long Term Ecological Research project website (www.mcmlter.org). Methods for upward looking image processing are available upon request from the author. This research was supported by the NASA ASTEP program (grant NNX07AM88G) and Office of Polar Programs (grants 9810219, 0096250, 0832755, 1041742, and 1115245). Logistical support was provided by the US Antarctic Program through funding from NSF.

References

Adams, E. E., J. C. Priscu, C. H. Fritsen, S. R. Smith, and S. L. Brackman (1998), Permanent ice covers of the McMurdo Dry Valley lakes, Antarctica: Bubble formation and metamorphism, in *Ecosystem Dynamics in a Polar Desert; the McMurdo Dry Valleys, Antarctica*, edited by J. C. Priscu, pp. 281–295, AGU, Washington, D. C.

Chinn, T. J. (1993), Physical hydrology of the dry valley lakes, in *Physical and Biogeochemical Processes in Antarctic Lakes*, edited by W. J. Green and E. I. Friedmann, pp. 1–51, AGU, Washington, D. C.

Clow, G. D., C. P. McKay, G. M. Simmons Jr., and R. A. Wharton Jr. (1988), Climatological observations and predicted sublimation rates at Lake Hoare, Antarctica, *J. Clim.*, *1*, 715–728.

Dana, G. L., R. A. J. Wharton, and R. Dubayah (1998), Solar radiation in the McMurdo Dry Valleys, Antarctica, in *Ecosystem Dynamics in a Polar Desert: The McMurdo Dry Valleys, Antarctica*, edited by J. P. Priscu, pp. 39–64, AGU, Washington, D. C.

Doran, P. T., et al. (2002), Antarctic climate cooling and terrestrial ecosystem response, *Nature*, *415*(6871), 517–520.

Dugan, H. D., M. K. Obryk, and P. T. Doran (2013), Lake ice ablation rates from permanently ice-covered Antarctic lakes, *J. Glaciol.*, *59*(215), 491–498.

Fritsen, C. H., and J. C. Priscu (1999), Seasonal change in the optical properties of the permanent ice cover on Lake Bonney, Antarctica: Consequences for lake productivity and phytoplankton dynamics, *Limnol. Oceanogr.*, *44*(2), 447–454.

Jepsen, S. M., E. E. Adams, and J. C. Priscu (2010), Sediment melt-migration dynamics in perennial Antarctic lake ice, *Arct. Antarct. Alp. Res.*, *42*(1), 57–66.

Kong, W., W. Li, I. Romancova, O. Prasil, and R. M. Morgan-Kiss (2014), An integrated study of photochemical function and expression of a key photochemical gene (*psbA*) in photosynthetic communities of Lake Bonney (McMurdo Dry Valleys, Antarctica), *FEMS Microbiol. Ecol.*, *89*(2), 293–302.

Lizotte, M. P., and J. C. Priscu (1992), Photosynthesis irradiance relationships in phytoplankton from the physically stable water column of a perennially ice-covered lake (Lake Bonney, Antarctica), *J. Phycol.*, *28*(2), 179–185.

Lizotte, M. P., and J. C. Priscu (1994), Natural fluorescence and quantum yields in vertically stationary phytoplankton from perennially ice-covered lakes, *Limnol. Oceanogr.*, *39*(6), 1399–1410.

Lizotte, M. P., T. R. Sharp, and J. C. Priscu (1996), Phytoplankton dynamics in the stratified water column of Lake Bonney, Antarctica. I. Biomass and productivity during the winter-spring transition, *Polar Biol.*, *16*(3), 155–162.

McKay, C. P., G. D. Clow, R. A. Wharton, and S. W. Squyres (1985), Thickness of ice on perennially frozen lakes, *Nature*, *313*(6003), 561–562.

McKay, C. P., G. D. Clow, D. T. Andersen, and R. A. Wharton (1994), Light transmission and reflection in perennially ice-covered Lake Hoare, Antarctica, *J. Geophys. Res.*, *99*(C10), 20,427–20,444, doi:10.1029/94JC01414.

Miskiewicz, E., A. G. Ivanov, J. P. Williams, M. U. Khan, S. Falk, and N. P. A. Huner (2000), Photosynthetic acclimation of the filamentous cyanobacterium, Plectonema boryanum UTEX 485, to temperature and light, *Plant Cell Physiol.*, *41*(6), 767–775.

Morgan-Kiss, R. M., J. C. Priscu, T. Pocock, L. Gudynaite-Savitch, and N. P. A. Huner (2006), Adaptation and acclimation of photosynthetic microorganisms to permanently cold environments, *Microbiol. Mol. Biol. Rev.*, *70*(1), 222–252.

Neale, P. J., and J. C. Priscu (1995), The photosynthetic apparatus of phytoplankton from a perennially ice-covered Antarctic Lake: Acclimation to an extreme shade environment, *Plant Cell Physiol.*, *36*(2), 253–263.

Nedell, S. S., D. W. Andersen, S. W. Squyres, and F. G. Love (1987), Sedimentation in ice-covered Lake Hoare, Antarctica, *Sedimentology*, *34*, 1093–1106.

Priscu, J. C. (1995), Phytoplankton nutrient deficiency in lakes of the Mcmurdo dry valleys, Antarctica, *Freshwater Biol.*, *34*(2), 215–227.

Priscu, J. C., C. H. Fritsen, E. E. Adams, S. J. Giovannoni, H. W. Paerl, C. P. McKay, P. T. Doran, D. A. Gordon, B. D. Lanoil, and J. L. Pinckney (1998), Perennial Antarctic lake ice: An oasis for life in a polar desert, *Science*, *280*(5372), 2095–2098.

Shibata, T., S. C. Tripathy, and J. Ishizaka (2010), Phytoplankton pigment change as a photoadaptive response to light variation caused by tidal cycle in Ariake Bay, Japan, *J. Oceanogr.*, *66*(6), 831–843.

Simmons, G. M., Jr., R. A. Wharton Jr., C. P. McKay, S. Nedell, and G. Clow (1986), Sand/ice interactions and sediment deposition in perenially ice-covered Antarctic lakes, *Antarct. J. U. S.*, *21*, 217–220.

Spigel, R. H., and J. C. Priscu (1998), Physical limnology of the McMurdo Dry Valley lakes, in *Ecosystem Dynamics in a Polar Desert: The McMurdo Dry Valleys, Antarctica*, edited by J. C. Priscu, pp. 153–187, AGU, Washington, D. C.

Spigel, R. H., I. Forne, and I. Sheppard (1991), Differences in temperature and conductivity between the east and west lobes of Lake Bonney: Evidence for circulation within and between lobes, *Antarct. J. U. S.*, *26*, 221–222.

Squyres, S. W., D. W. Andersen, S. S. Nedell, and J. R. A. Wharton (1991), Lake Hoare, Antarctica: Sedimentation through thick perennial ice cover, *Sedimentology*, *38*, 363–380.

Stone, W., et al. (2010), Design and deployment of a four-degrees-of-freedom hovering autonomous underwater vehicle for sub-ice exploration and mapping, *Eng. Marit. Environ.*, *224*, 341–361.

Tanabe, Y., S. Kudoh, S. Imura, and M. Fukuchi (2008), Phytoplankton blooms under dim and cold conditions in freshwater lakes of East Antarctica, *Polar Biol.*, *31*(2), 199–208.

Vincent, A. C., D. R. Mueller, and W. F. Vincent (2008), Simulated heat storage in a perennially ice-covered high Arctic lake: Sensitivity to climate change, *J. Geophys. Res.*, *113*, C04036, doi:10.1029/2007JC004360.

Wilson, A. T. (1981), A review of the geochemistry and lake physics of the antarctic dry areas, in *Dry Valley Drilling Project*, edited by L. D. McGinnis, pp. 185–192, AGU, Washington, D. C.